Vietnam Journal of Mechanics, Vol. 47, No. 4 (2025), pp. 293 – 304
DOI: https://doi.org/10.15625/0866-7136/20921

GEOMETRIC INFLUENCE OF ENTRY ANGLE AND CONTRACTION RATIO ON DROPLET REGIME TRANSITION FROM TRAP TO SQUEEZE IN MICROCHANNEL

Van Thanh Hoang*, Thanh Tung Nguyen, Hong Vinh Pham
Department of Mechanical Engineering, The University of Danang - University of Science and Technology, 54 Nguyen Luong Bang street, Danang City 50000, Vietnam
*E-mail: hvthanh@dut.udn.vn

Received: 09 June 2024 / Revised: 08 June 2025 / Accepted: 14 July 2025
Published online: 09 August 2025

Abstract. To precisely control and manipulate the main droplet within a microfluidic system, aside from modifying the flow characteristics and liquid properties, the geometric design of the microchannel also plays a crucial role in the droplet dynamics. Three main regimes are observed in a droplet in a contraction microchannel: trap, squeeze, and breakup. This study employs theoretical and three-dimensional numerical models to assess how two geometric parameters of the microchannel, namely the entry angle (α) and the contraction ratio (C), influence the critical capillary number (Ca) for droplet dynamics of trap-squeeze regime transition. The model's predictions align perfectly with simulation results. Additionally, the study investigates the impact of the entry angle on droplet deformation.

Keywords: capillary number, microfluidic, contraction ratio, numerical model, entry geometry.

1. INTRODUCTION

The evolution of droplet-based microfluidic systems represents a significant advancement in technology, driving the development of innovative experimental methodologies. These systems offer distinct advantages including rapid processing, minimal sample and reagent usage, straightforward operation, and precise manipulation capabilities. As a result, they not only enhance cost-effectiveness and time efficiency but also facilitate widespread applications across biomedical research, chemistry, and beyond [1–3].

Contraction microchannels are utilized in various engineering applications such as DNA analysis [4], emulsification [5], cell filtration [6], and material property analysis [7]. Consequently, the study of droplet dynamics in contraction microchannels has garnered significant interest from researchers. For instance, Zang et al. investigated the deformation of small droplets passing through narrow microchannels [8]. Mulligan and Rothstein conducted experiments to evaluate droplet behavior, including deformation and breakup, in hyperbolic microchannels [9]. In recent years, the behavior of droplets in contraction microchannels has been extensively studied. Hoang et al. examined the effects of contraction ratio (C) and capillary number (Ca) on droplet behavior through numerical simulations [10]. The geometric effects of microchannel width ratio were thoroughly studied by Do et al. [11]. Recently, they also considered the influence of the contact angle (θ) between droplets and the channel walls on droplet dynamics [12].

With technological advancements, numerical simulations have emerged as valuable tools for studying droplet dynamics [13–15]. However, previous studies often relied on 2D numerical simulations [16, 17]. The discrepancies between 2D numerical simulations and experimental results have been highlighted in many studies, especially for non-circular microchannels [18, 19]. Consequently, 3D numerical simulations are gradually replacing 2D simulations.

This study uses a 3D numerical model to simulate and assess how three parameters simultaneously affect droplet behavior, particularly in the trap and squeeze regimes: capillary number (Ca), entry angle (α), and contraction ratio (C). A theoretical model is suggested to predict when these two regimes will change. Additionally, the deformation of droplets due to the influence of the entry angle (α) is also considered. This research provides a comprehensive understanding of droplet dynamics in microfluidic systems and is valuable for the geometric design of microchannels.

2. NUMERICAL MODEL

2.1. Geometric characteristics and boundary conditions

A system of contraction microchannels with specific geometric characteristics is shown in Fig. 1. The larger microchannel and the contraction microchannel are the two main components of this system. The coordinate axis center is occupied by a droplet of diameter D. The larger microchannel has dimensions of $3D$ length and $2D$ width, whereas the constricted microchannel has dimensions of $15D$ length and W width. The microchannel depth of $2.5D$ is chosen in order to reduce the impact of sidewall deformations on droplet behavior [20–22]. The contraction microchannel's entry angle is represented by the symbol α. During the simulation, the contraction ratio (C) is adjusted by changing the width of the contraction microchannel, defined as $C = D/W$. These

geometric parameters have been validated and are commonly used to assess droplet deformation and dynamics in contraction microchannels [10, 13, 23].

The droplet and continuous phase exhibit the characteristics of an incompressible Newtonian fluid, specifically a water phase with viscosity μ_d, while the continuous phase is an oil with viscosity μ_c. There is a fixed viscosity ratio (μ_d/μ_c) of 0.15. The continuous phase's velocity is set at 0.00085 m/s, and the outlet pressure is zero. The capillary number (Ca), representing the surface force, is defined as $Ca = \mu_c v/\sigma$, where σ is the surface tension. To vary the capillary number, σ is adjusted during the simulation. The microchannel walls have a contact angle of 180° with the droplet and exhibit no slip.

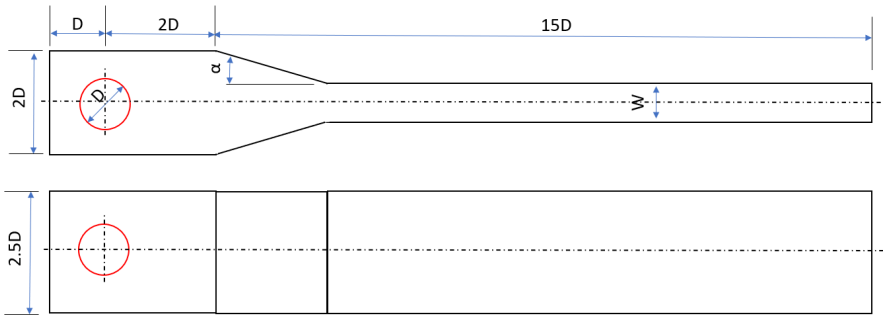

Fig. 1. Details of the contraction microchannel geometry

2.2. Simulation setup

The simulations are carried out using CFD software. The study uses various computational techniques, such as the PISO algorithm, the PRESTO! method, a Second-Order Upwind Scheme, and the Geo-Reconstruct scheme. Grid size significantly influences droplet behavior [24]. In this study, a grid size of $W/30$ is used, which has been validated as effective in numerical simulations of droplet dynamics in microchannels and has been widely adopted [25]. The Courant number, which determines the computational time step, is set to 0.25, consistent with previous studies [10–12, 23, 25]. Considering the symmetry of the model, a quarter-symmetry model is used to reduce the computational cost of the simulations, as detailed in Fig. 2.

3. PREDICTION THEORY MODEL

Droplet motion within a microchannel with a contraction undergoes three typical regimes: trap, squeeze, and breakup, detailed in Fig. 3. According to Hoang et al. [24], entry angle was found to be significant for the transition from trap to squeeze. Therefore, this study focuses on the trap-squeeze regimes for various contraction ratio and entry angle.

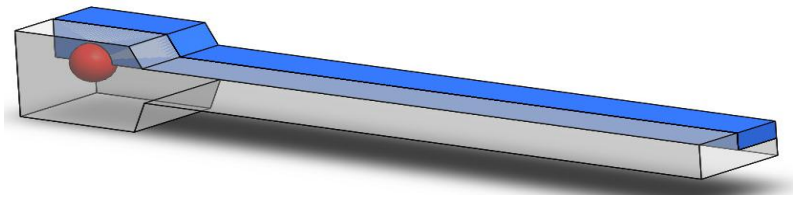

Fig. 2. Quarter-symmetry model (blue)

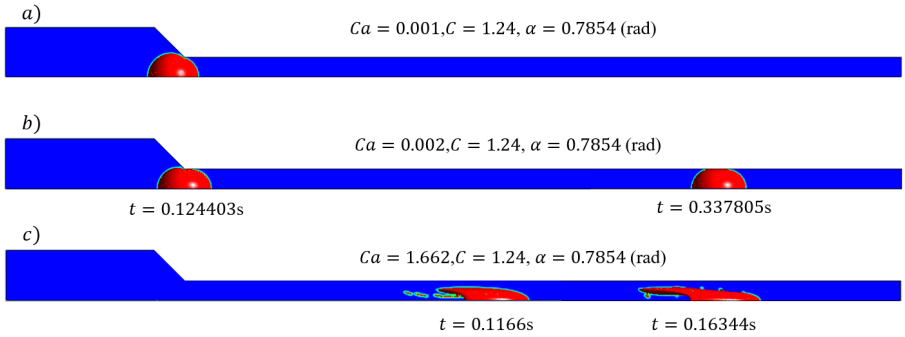

Fig. 3. Three classical droplet regimes in contraction microchannels: (a) trap, (b) squeeze, and (c) breakup

Considering the scenario of a water droplet being trapped, at this position, the droplet is subjected to the influence of hydrostatic pressure. The hydrostatic pressure Δp_h can be represented as follows

$$\Delta p_h = \frac{\mu_m V_i C_f L_i}{2D_h^2}, \tag{1}$$

where the friction coefficient is denoted as $C_f = 57.7$ and D_h is the hydraulic diameter [26].

The Laplace pressure for a given interface is defined by the Young–Laplace equation as $\Delta p = \dfrac{2\sigma}{R}$. When the droplet moves into the contraction microchannel, the droplet loses its original spherical shape as it is trapped, as shown in Fig. 4, which causes a discrepancy in radii between the droplet's front and back interfaces. The Laplace pressures at the back and front interfaces of the droplet are Δp_b and Δp_f, respectively. As a result, $\Delta p = \Delta p_f - \Delta p_b$ is the pressure difference between the front and back of the droplet, where $\Delta p_b = \sigma\left(\dfrac{1}{R_{y,b}} + \dfrac{1}{R_{z,b}}\right)$, and $\Delta p_f = \sigma\left(\dfrac{1}{R_{y,f}} + \dfrac{1}{R_{z,f}}\right)$ are the Laplace pressures at the back and the front interfaces of the droplet, respectively; R_y and R_z are the radii of curvature of the droplet in the y and z directions, respectively, and the subscripts b and f stand for

curvature radii measured at the back and the front of the droplet, respectively, as shown in Fig. 4(a).

Due to the height of the large microchannel is equal to that of the contraction microchannel, one can assume that $R_{y,f} = R_{y,b}$, thus, the radii of the interface are considered in the z direction only. Consequently, Δp can be simplified in Eq. (2) with two characteristic radii, R_b and R_f, which correspond to its front and back interfaces as depicted in Fig. 4(b) [10]

$$\Delta p = \sigma \left(\frac{1}{R_f} - \frac{1}{R_b} \right). \tag{2}$$

For the back radius R_b, it is influenced by the entry angle α [24]. Thus, R_b increases with increasing α and is independent of the contraction ratio C, so R_b can be approximated as $R_b \sim R_\alpha$. However, the front radius R_f, which is defined as $R_f \sim RC^{-M}$, may rely on the contraction ratio C even though it is thought to be independent of α. As a result, the pressure differential between the droplet's front and back interfaces is shown as follows

$$\Delta p = \frac{\sigma}{R} \left(A_0 C^M - \frac{A_1}{\alpha} \right), \tag{3}$$

where A_0, A_1, and M are constants. If $\Delta p_h < \Delta p$, the droplet will be trapped. Therefore, the following formula is used to find the critical capillary number for droplet dynamics of trap-squeeze regime transition

$$Ca_c > \frac{2{D_h}^2}{C_f L_i R} \left(A_0 C^M - \frac{A_1}{\alpha} \right). \tag{4}$$

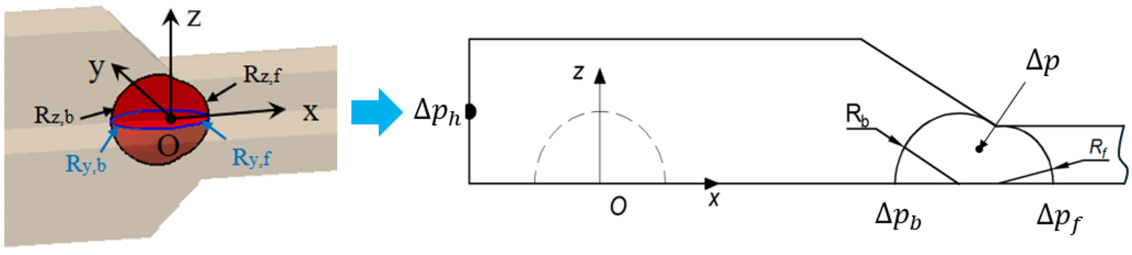

Fig. 4. Diagram illustrating the mechanism of the trap due to the impact of entry angle and contraction ratio: (a) Full description, (b) simplified analysis

4. RESULTS AND DISCUSSION

4.1. Trap to squeeze

Fig. 5 illustrates the detailed results from the predictive equation (4) and the simulation outcomes. The solid lines represent the critical capillary numbers for the droplet dynamics transition from the trap to the squeeze regime, calculated using the predictive equation (4) with newly determined constants: $M = 3.0067$, $A_0 = 0.0084$, and $A_1 = 0.0016$. The dashed lines show predictions using the constants from Hoang et al. [24], which are: $M = 0.054$, $A_0 = 0.016$, and $A_1 = 0.001$.

The data points correspond to the critical capillary numbers at various entry angles for three different contraction ratios: $C = 1.11$, $C = 1.25$, and $C = 1.43$. The new constants closely match the simulation results across all three C values, accurately reflecting the transition behavior for each contraction ratio. However, with the constants from Hoang et al. [24], the predicted results appear nearly identical across the three contraction ratios, with minimal distinction between them, leading to lower accuracy when the contraction ratio varies.

This comparison highlights that the newly determined constants enable the model to better reflect the differences in droplet dynamics across each contraction ratio. The figure also shows that as the contraction ratio increases, the critical capillary number required for the regime transition also rises, emphasizing the importance of geometric adjustments in influencing droplet dynamics and optimizing microfluidic applications.

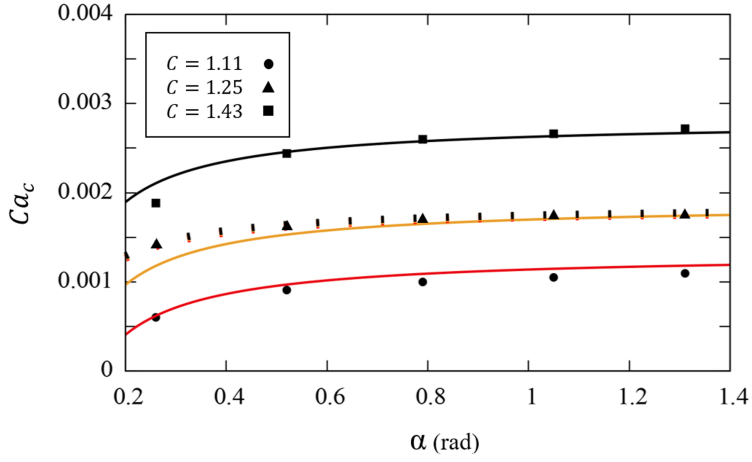

Fig. 5. Effects of entry angle and contraction ratio on the critical capillary number. Solid and dashed lines represent predictions using current constants and constants from Hoang et al. [24], respectively. Colors indicate contraction ratios: red ($C = 1.11$), yellow ($C = 1.25$), and black ($C = 1.43$)

To examine this more closely, the critical capillary number is fixed at $Ca = 0.0015$, and the entry angle and contraction ratio are varied to investigate droplet regimes. The simulation results and predictive model are detailed in Fig. 6. The trend indicates that with a smaller entry angle, a larger contraction ratio is required for the droplet to be trapped. Conversely, as the entry angle increases, the required contraction ratio decreases.

Furthermore, the consistency between the predictive model and the simulation results across different contraction ratios and entry angles reinforces the reliability of the model. This validation is critical for designing and optimizing microfluidic systems, particularly in applications where precise droplet manipulation is essential. The results presented in Figs. 5 and 6 not only validate the theoretical model but also underscore the importance of considering both the entry angle and contraction ratio in microchannel design to achieve desired droplet behavior. The high degree of correlation between the model and simulation results indicates that this approach can be confidently used to predict and control droplet transitions in various microfluidic applications.

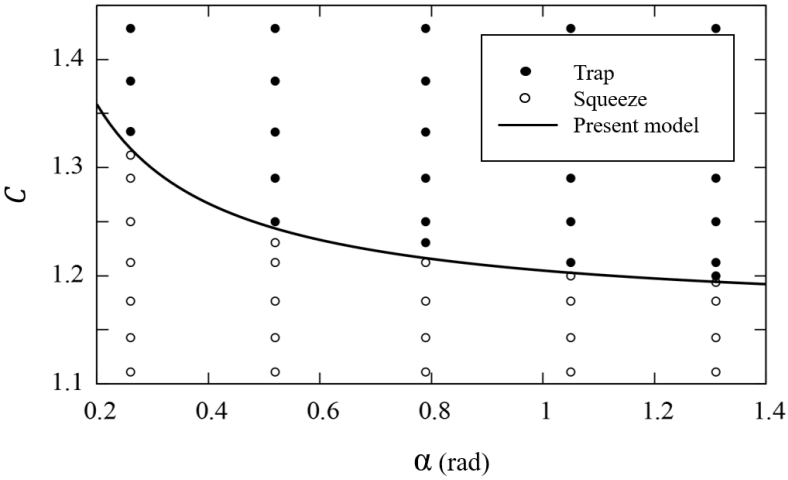

Fig. 6. Phase diagram of regimes with different values of entry angle and contraction ratio with $Ca = 0.0015$

4.2. Pressure differences in trap and squeeze regimes

As outlined in the theoretical framework, the flow pressure and the internal pressure of the droplet are the key factors that determine the droplet's regime. This section compares the pressure characteristics of the trap and squeeze regimes under the following conditions: contraction ratio $C = 1.25$, entry angle $\alpha = 0.7854$, capillary number $Ca = 0.001$ for the trap regime, and $Ca = 0.002$ for the squeeze regime.

Fig. 7 shows a clear difference in the internal pressure of the droplet between the two regimes. In the trap regime (i.e., low Ca), the internal pressure of the droplet increases significantly as Ca increases, highlighting the role of surface tension in controlling droplet pressure. As the droplet passes through the constriction, the pressure distribution around it becomes asymmetric, with the pressure in front of the droplet being higher than behind it. This pressure difference is larger at low Ca and can exceed the inlet pressure of the flow, resulting in the trap regime.

Fig. 8 illustrates the variation of inlet pressure (Pa_{in}) between the two regimes. At higher Ca, the droplet moves faster [23]. As the droplet enters the constricted region, the inlet pressure increases to push the droplet into the contraction microchannel. Once the inlet pressure becomes large enough to overcome the pressure difference across the droplet, it is squeezed into the constriction, and this pressure level is maintained throughout the droplet's motion in the contraction microchannel.

In contrast, in the trap regime, although the inlet pressure increases and reaches a peak value, it remains insufficient to overcome the internal pressure of the droplet. As a result, the droplet is pushed back, allowing the carrier fluid to flow into the contraction microchannel, causing the pressure to drop. The flow then continues to push the droplet forward, increasing the inlet pressure again, but subsequent peaks are lower than the initial one. Eventually, the system reaches a steady state, where the droplet remains trapped and the inlet pressure stabilizes. Notably, this stabilized pressure level is similar in both regimes.

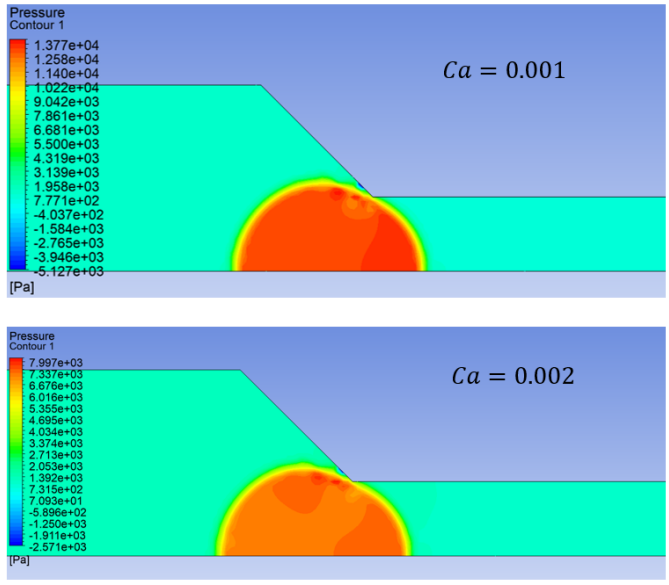

Fig. 7. Comparison of internal droplet pressure in trap and squeeze regimes

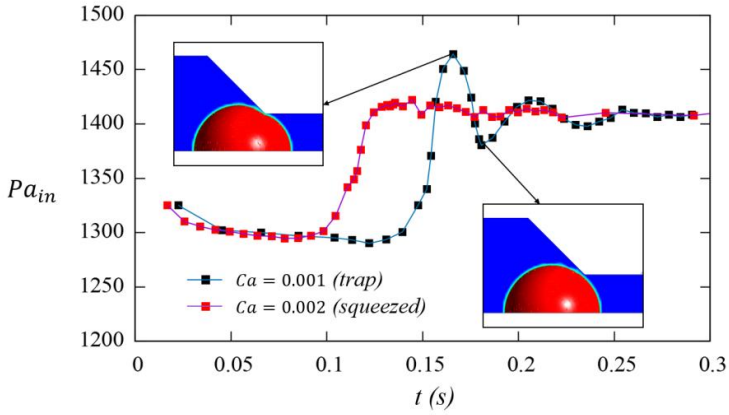

Fig. 8. Variation of inlet pressure during droplet entry into the constriction in trap and squeeze regimes

4.3. Droplet deformation

The droplet must deform in order to enter the contraction microchannel; its shape is determined by the contraction ratio (C), viscosity ratio (λ), and capillary number (Ca) [11, 12]. To assess the droplet deformation due to the impact of the entry angle (α), the maximum length of the droplet ($L_{\max}$) deformed before entering the contraction microchannel is considered.

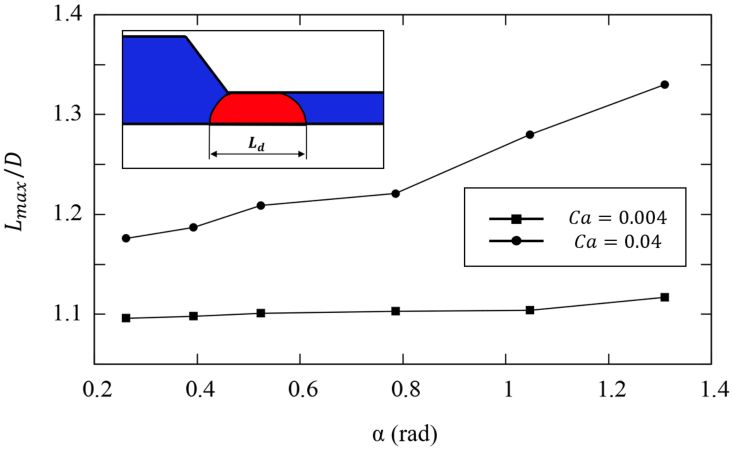

Fig. 9. Entry angle's effects on the maximum droplet length ratio with $C = 1.25$

Fig. 9 illustrates the maximum droplet length ratio ($L_{\max}/D$) as a function of the entry angle (α) when the droplet passes through a constricted microchannel under two different capillary numbers: $Ca = 0.04$ and $Ca = 0.004$. The results indicate that as the entry angle increases, the maximum droplet length ratio also increases significantly

for $Ca = 0.04$. This trend suggests that larger entry angles lead to greater elongation of the droplet at higher capillary numbers, highlighting the pronounced effect of the entry angle on droplet deformation under these conditions. Conversely, for $Ca = 0.004$, the droplet length ratio remains relatively stable across varying entry angles, indicating minimal influence of the entry angle on droplet deformation at lower capillary numbers. These findings emphasize the importance of considering both the entry angle and the capillary number in microchannel design, particularly for applications requiring precise control over droplet deformation. Larger entry angles and higher capillary numbers need careful management to avoid excessive elongation, which could impact the functionality of the droplet in various microfluidic processes.

5. CONCLUSION

This study has effectively elucidated the intricate relationship between entry angle (α) and contraction ratio (C) in microfluidic systems using both 3D simulations and theoretical modeling. The predictive modeling approach has rigorously validated its accuracy in forecasting the critical capillary number (Ca) necessary for droplet dynamics of trap-squeeze regime transition. These results not only provide a solid foundation but also underscore the importance of these parameters in optimizing microfluidic system designs for a wide range of critical applications. The findings highlight the potential for further advancements in understanding and manipulating droplet dynamics within microchannels, paving the way for enhanced efficiency and innovation in microfluidic technology.

DECLARATION OF COMPETING INTEREST

The authors declare that they have no known competing financial interests or personal relationships that could have appeared to influence the work reported in this paper.

ACKNOWLEDGMENT

Thanh Tung Nguyen was funded by the Master, PhD Scholarship Programme of Vingroup Innovation Foundation (VINIF), code VINIF.2023.ThS.118.

REFERENCES

[1] J. Castillo-Leon and W. E. Svendsen. *Lab-on-a-chip devices and micro-total analysis systems: A practical guide*. Springer International Publishing, (2015). https://doi.org/10.1007/978-3-319-08687-3.

[2] E. Y. Basova and F. Foret. Droplet microfluidics in (bio)chemical analysis. *The Analyst*, **140**, (1), (2015), pp. 22–38. https://doi.org/10.1039/c4an01209g.

[3] J. H. Xu, J. Tan, S. W. Li, and G. S. Luo. Enhancement of mass transfer performance of liquid–liquid system by droplet flow in microchannels. *Chemical Engineering Journal*, **141**, (2008), pp. 242–249. https://doi.org/10.1016/j.cej.2007.12.030.

[4] G. C. Randall, K. M. Schultz, and P. S. Doyle. Methods to electrophoretically stretch DNA: microcontractions, gels, and hybrid gel-microcontraction devices. *Lab on a Chip*, **6**, (4), (2006), pp. 516–525. https://doi.org/10.1039/b515326c.

[5] S. L. Anna, N. Bontoux, and H. A. Stone. Formation of dispersions using "flow focusing" in microchannels. *Applied Physics Letters*, **82**, (2003), pp. 364–366. https://doi.org/10.1063/1.1537519.

[6] Z. Zhang, J. Xu, B. Hong, and X. Chen. The effects of 3D channel geometry on CTC passing pressure – towards deformability-based cancer cell separation. *Lab on a Chip*, **14**, (14), (2014), pp. 2576–2584. https://doi.org/10.1039/c4lc00301b.

[7] C. J. Pipe and G. H. McKinley. Microfluidic rheometry. *Mechanics Research Communications*, **36**, (2009), pp. 110–120. https://doi.org/10.1016/j.mechrescom.2008.08.009.

[8] Z. Zhang, X. Chen, and J. Xu. Entry effects of droplet in a micro confinement: Implications for deformation-based circulating tumor cell microfiltration. *Biomicrofluidics*, **9**, (2015). https://doi.org/10.1063/1.4916645.

[9] M. K. Mulligan and J. P. Rothstein. Deformation and breakup of micro- and nanoparticle stabilized droplets in microfluidic extensional flows. *Langmuir*, **27**, (2011), pp. 9760–9768. https://doi.org/10.1021/la201523r.

[10] V. T. Hoang, J. Lim, C. Byon, and J. M. Park. Three-dimensional simulation of droplet dynamics in planar contraction microchannel. *Chemical Engineering Science*, **176**, (2018), pp. 59–65. https://doi.org/10.1016/j.ces.2017.10.020.

[11] L. H. T. Do, T. T. Nguyen, V. T. Hoang, and M. S. Tran. Geometric influence of width ratio and contraction ratio on droplet dynamics in microchannel using a 3D numerical simulation. *Heat Transfer*, **53**, (2024), pp. 2934–2947. https://doi.org/10.1002/htj.23066.

[12] L. H. T. Do, T. T. Nguyen, V. T. Hoang, and J.-W. Lee. Simultaneous influence of contact angle, capillary number, and contraction ratio on droplet dynamics in hydrophobic microchannel. *Fluid Dynamics Research*, **56**, (2024). https://doi.org/10.1088/1873-7005/ad4a2b.

[13] D. J. E. Harvie, M. R. Davidson, J. J. Cooper-White, and M. Rudman. A parametric study of droplet deformation through a microfluidic contraction. *ANZIAM Journal*, **46**, (2005). https://doi.org/10.21914/anziamj.v46i0.953.

[14] V. T. Hoang, T. T. Nguyen, B.-T. Truong-Le, and T. A. Vo. Simultaneous effects of capillary number, viscosity ratio, and contraction ratio on droplet dynamics in contraction microchannel. *Journal of Micromechanics and Microengineering*, **34**, (2024). https://doi.org/10.1088/1361-6439/ad6f1b.

[15] T. T. Nguyen and V. T. Hoang. Regime dynamics of droplet behavior in hydrophilic contraction microchannel. *Chemical Papers*, **79**, (2025), pp. 2337–2345. https://doi.org/10.1007/s11696-025-03928-6.

[16] R. E. Khayat, A. Luciani, and L. A. Utracki. Boundary-element analysis of planar drop deformation in confined flow. Part 1. Newtonian fluids. *Engineering Analysis with Boundary Elements*, **19**, (1997), pp. 279–289. https://doi.org/10.1016/s0955-7997(97)00040-4.

[17] C.-K. Chung, J.-M. Kim, K.-H. Ahn, and S.-J. Lee. Numerical study on the effect of viscoelasticity on pressure drop and film thickness for a droplet flow in a confined microchannel. *Korea-Australia Rheology Journal*, **21**, (1), (2009), pp. 59–69.

[18] I.-L. Ngo, T.-D. Dang, C. Byon, and S. W. Joo. A numerical study on the dynamics of droplet formation in a microfluidic double T-junction. *Biomicrofluidics*, **9**, (2015). https://doi.org/10.1063/1.4916228.

[19] D. J. E. Harvie, J. J. Cooper-White, and M. R. Davidson. Deformation of a viscoelastic droplet passing through a microfluidic contraction. *Journal of Non-Newtonian Fluid Mechanics*, **155**, (2008), pp. 67–79. https://doi.org/10.1016/j.jnnfm.2008.05.002.

[20] N. Ioannou, H. Liu, and Y. H. Zhang. Droplet dynamics in confinement. *Journal of Computational Science*, **17**, (2016), pp. 463–474. https://doi.org/10.1016/j.jocs.2016.03.009.

[21] S. Guido and M. Villone. Three-dimensional shape of a drop under simple shear flow. *Journal of Rheology*, **42**, (1998), pp. 395–415. https://doi.org/10.1122/1.550942.

[22] M. R. Kennedy, C. Pozrikidis, and R. Skalak. Motion and deformation of liquid drops, and the rheology of dilute emulsions in simple shear flow. *Computers & Fluids*, **23**, (1994), pp. 251–278. https://doi.org/10.1016/0045-7930(94)90040-x.

[23] T. T. Nguyen, V. T. Hoang, D. B. Luu, N. H. Tran, M. S. Tran, and L. H. T. Do. Study on the velocity of droplet at steady state in contraction microchannels by numerical simulation. *Vietnam Journal of Mechanics*, **45**, (2023), pp. 287–295. https://doi.org/10.15625/0866-7136/18918.

[24] V. T. Hoang, V. D. Le, J. M. Park, and B.-T. Truong-Le. Effect of entry geometry on droplet dynamics in contraction microchannel. *International Journal of Multiphase Flow*, **167**, (2023). https://doi.org/10.1016/j.ijmultiphaseflow.2023.104543.

[25] X.-B. Li, F.-C. Li, J.-C. Yang, H. Kinoshita, M. Oishi, and M. Oshima. Study on the mechanism of droplet formation in T-junction microchannel. *Chemical Engineering Science*, **69**, (2012), pp. 340–351. https://doi.org/10.1016/j.ces.2011.10.048.

[26] B. R. Munson, D. F. Young, and T. H. Okiishi. Fundamentals of fluid mechanics. *Oceanographic Literature Review*, **10**, (42), (1995).